


# Comparison of FY-4A/AGRI SST with Himawari-8/AHI and In Situ SST

Chang Yang <sup>1</sup>, Lei Guan <sup>1,2,3,\*</sup>  and Xiaohui Sun <sup>1,3</sup>

<sup>1</sup> College of Marine Technology, Faculty of Information Science and Engineering, Ocean University of China, Qingdao 266100, China; yangchang@stu.ouc.edu.cn (C.Y.); sunxiaohui@stu.ouc.edu.cn (X.S.)

<sup>2</sup> Laboratory for Regional Oceanography and Numerical Modeling, Qingdao National Laboratory for Marine Science and Technology, Qingdao 266237, China

<sup>3</sup> Key Laboratory of Ocean Observation and Information of Hainan Province, Sanya Oceanographic Institution, Ocean University of China, Sanya 572024, China

\* Correspondence: leiguan@ouc.edu.cn; Tel.: +86-0532-66781802

**Abstract:** The Fengyun-4A (FY-4A) satellite is a new-generation geostationary meteorological satellite developed by China. The advanced geosynchronous radiation imager (AGRI), one of the key payloads onboard FY-4A, can monitor sea surface temperature (SST). This paper compares FY-4A/AGRI SST with in situ and Himawari-8/advanced Himawari imager (AHI) SST. The study area spans 30°E–180°E, 60°S–60°N, and the study period is from January 2019 to December 2021. The matching time window of the three data is 30 min, and the space window is 0.1°. The quality control criterion is to select all clear sky and well-distributed matchups within the study period, removing the influence of SST fronts. The results of the difference between FY-4A/AGRI and in situ SST show a bias of  $-0.12$  °C, median of  $-0.05$  °C, standard deviation (STD) of  $0.76$  °C, robust standard deviation (RSD) of  $0.68$  °C, and root mean square error (RMSE) of  $0.77$  °C for daytime and a bias of  $0.00$  °C, median of  $0.05$  °C, STD of  $0.78$  °C, RSD of  $0.72$  °C, and RMSE of  $0.78$  °C for nighttime. The results of the difference between FY-4A/AGRI SST and Himawari-8/AHI SST show a bias of  $0.04$  °C, median of  $0.10$  °C, STD of  $0.78$  °C, RSD of  $0.70$  °C, and RMSE of  $0.78$  °C for daytime and the bias of  $0.30$  °C, median of  $0.34$  °C, STD of  $0.81$  °C, RSD of  $0.76$  °C, and RMSE of  $0.86$  °C for nighttime. The three-way error analysis also indicates a relatively larger error of AGRI SST. Regarding timescale, the bias and STD of FY-4A/AGRI SST show no seasonal correlation, but FY-4A/AGRI SST has a noticeable bias jump in the study period. Regarding spatial scale, FY-4A/AGRI SST shows negative bias at the edge of the AGRI SST coverage in the Pacific region near 160°E longitude and positive bias in high latitudes of the southern hemisphere. The accuracy of FY-4A/AGRI SST depends on the satellite zenith angle and water vapor. Further research on the FY-4A/AGRI SST retrieval algorithm accounting for the variability of water vapor will be conducted.

**Keywords:** sea surface temperature; FY-4A; AGRI; Himawari-8; AHI



**Citation:** Yang, C.; Guan, L.; Sun, X. Comparison of FY-4A/AGRI SST with Himawari-8/AHI and In Situ SST. *Remote Sens.* **2023**, *15*, 4139. <https://doi.org/10.3390/rs15174139>

Academic Editor: Yukiharu Hisaki

Received: 4 July 2023

Revised: 17 August 2023

Accepted: 21 August 2023

Published: 23 August 2023



**Copyright:** © 2023 by the authors. Licensee MDPI, Basel, Switzerland. This article is an open access article distributed under the terms and conditions of the Creative Commons Attribution (CC BY) license (<https://creativecommons.org/licenses/by/4.0/>).

## 1. Introduction

Sea surface temperature (SST) is one of the most important variables to monitor ocean processes and climate change. The acquisition of SST with high spatial and temporal resolution, high precision, and large range is of great significance to the study of climate change and marine phenomena, such as ocean circulation, mesoscale vortices, upwelling, and seawater mixing [1,2]. The Global Climate Observing System declared SST a critical climate variable [3]. The accuracy of most satellite SST data for marine and atmospheric applications is about  $0.5$  °C [3], and SST data for climate change monitoring is higher, which should be less than  $0.1$  °C [3].

The SST observations in the infrared band are mostly by the geostationary orbiting satellites and sun-synchronous polar orbiting satellites. Compared with polar-orbiting

satellites, SST observation from geostationary orbit is characterized by higher time resolution. It can obtain a large-scale diurnal variation of SST, which has important advantages in observing SST change. SST data from different sensors onboard satellites vary greatly in data format and error, and data quality is uncertain. Therefore, it is necessary to carefully evaluate the accuracy of SST data from different sources before applying SST data.

The first Geostationary Operational Environmental Satellite (GOES) was launched in October 1975 as a joint effort of the National Oceanic and Atmospheric Administration (NOAA) and the National Aeronautics and Space Administration (NASA). The visible, infrared spin-scan radiometer (VISSR) onboard the GOES-1/2/3 had an infrared channel in the 10.5–12.6  $\mu\text{m}$ . Since only one infrared channel existed, the SST could not be retrieved using the split-window atmospheric correction algorithm [4]. The VISSR atmospheric sounding instrument (VAS) is a payload onboard GOES-5, 3.9, 11, and 12  $\mu\text{m}$  channels of VAS that can generate SSTs with an accuracy of 0.9–1.0  $^{\circ}\text{C}$  compared with the buoy data, firstly demonstrating the ability to retrieve SSTs from a geostationary satellite [5,6]. The GOES Imager with five channels had flown on the GOES 8–15 satellites, 3.9, 10.7 and 11.95  $\mu\text{m}$  channels of the GOES Imager onboard GOES 8/9/10/11 can be used for SST retrieval [6]. GOES-8, launched in May 1994 for the first time, provided SST with similar accuracy to polar orbiting satellites and improved the spatial resolution compared with the earlier GOES [7]. GOES-12 became operational in 2003, and the subsequent GOES 13/14/15 only had 3.9 and 10.7  $\mu\text{m}$  channels used to generate SSTs. The bias and STD were  $-0.53^{\circ}\text{C}$  and  $0.66^{\circ}\text{C}$  for daytime, and the bias and STD were  $-0.51^{\circ}\text{C}$  and  $0.89^{\circ}\text{C}$  for nighttime compared with drifting buoy SSTs [8]. The Advanced Baseline Imager (ABI) is a payload onboard GOES 16/17/18, a new generation stationary satellite imager developed by the United States [9,10]. 3.9, 8.5, 10.35, 11.2 and 12.3  $\mu\text{m}$  channels of ABI can be used for SST retrieval. The ABI SST algorithms were implemented within the Advanced Clear-Sky Processor for Oceans (ACSPO) [10,11]. Compared with in situ data, ABI had a bias of less than  $0.1^{\circ}\text{C}$  and the RMSE of  $0.5^{\circ}\text{C}$  in the Tropical and Southwestern Atlantic Ocean in 2018 [9]. Compared with M-AERIS SST from January 2018 to October 2019, ABI SST showed bias and RSD of  $0.086^{\circ}\text{C}$  and  $0.220^{\circ}\text{C}$ , respectively [12].

The Japan Meteorological Agency (JMA) launched the first Japanese geostationary meteorological satellite (GMS-1) in 1977, followed by GMS-2/3/4/5. The stretched-visible infrared spin scan radiometer (S-VISSR) onboard GMS-5 provided the SST product with an RMSE of  $0.8^{\circ}\text{C}$  compared with buoy data [13]. The Multifunctional Transport Satellite (MTSAT) is the second generation of the Japanese GMS series, including MTSAT-1 and MTSAT-2. Compared with drifting and moored buoy SST, the bias of MTSAT SST was close to  $0.0^{\circ}\text{C}$ , the RMSE was  $0.8^{\circ}\text{C}$ , and the RMSE was  $0.7^{\circ}\text{C}$  when the satellite zenith angle was  $<50^{\circ}$  [14]. The SST of the MTSAT-2 imager showed a bias and an STD of  $0.26^{\circ}\text{C}$  and  $0.48^{\circ}\text{C}$ , respectively, compared with in situ SST in the tropical Western Pacific from August to October 2015 [15]. Himawari-8 [16] is the latest generation of Japanese GMS launched on 7 October 2014, and put into operation in 2015. The advanced Himawari imager (AHI) onboard Himawari-8 consists of 16 observation channels (three visible, three near-infrared, and ten infrared channels). Channels of 3.9, 8.6, 10.4, 11.2, and 12.4  $\mu\text{m}$  can be used for SST retrieval [16]. Himawari-8/AHI SST product was developed by the Japan Aerospace Exploration Agency (JAXA) using a quasi-physical algorithm [17]. The RMSE and bias of AHI SST minus buoy SST from June to September 2015 were  $0.59^{\circ}\text{C}$  and  $-0.16^{\circ}\text{C}$ , respectively [17]. The Advanced Clear Sky Processor for Ocean (ACSPO) Himawari-8/AHI SST product derived by the NOAA ACSPO system, showed a bias within  $\pm 0.2^{\circ}\text{C}$  and STD of  $0.4$ – $0.6^{\circ}\text{C}$ , respectively, compared with in situ SST [18]. Himawari-8 AHI SST products also produced by the Australian Bureau of Meteorology for Australian applications [19]. Ditri et al. compared Himawari-8/AHI SST with buoy SST at TAO moorings and thermometers on the Great Barrier Reef in the tropical Western Pacific, showing that ACSPO Himawari-8/AHI SST was more consistent with in situ SST compared with MTSAT-2 SST [15]. Kusuma et al. conducted a comparative analysis of Aqua/Terra MODIS SST and JAXA Himawari-8/9 AHI SST in Indonesian water, and the

results showed a bias and an STD of 0.08 °C and 0.18 °C, respectively [20]. Sukresno et al. verified JAXA Himawari-8/AHI SST, buoy SST, and multiscale ultrahigh-resolution SST from December 2016 to July 2017, and the variances were 2.5 °C, 0.285 °C, and 1.21 °C, respectively [21]. When compared with in situ skin SSTs derived from shipboard Infrared SST Autonomous Radiometers in the Australian region from January 2016 to March 2017 by Yang et al., JAXA Himawari-8/AHI SST showed the bias and STD of 0.09 °C and 0.30 °C, respectively [22]. Compared with in situ SST, JAXA AHI SST had a bias and an RMSE between −0.11 °C and −0.03 °C and between 0.58 °C and 0.73 °C, respectively, from July 2015 to June 2017 [23]. Wang Peng et al. used the nonlinear SST algorithm (NLSST) to retrieve the Himawari-8/AHI SST under all weather conditions and verified it with buoy SST. The results showed an RMSE and a bias of 0.872 °C and −0.005 °C, respectively [24]. The bias and RMSE of JAXA Himawari-8/AHI SST minus buoy SST from July 2015 to May 2022 were 0.10 °C and 0.99 °C, respectively [25].

The Spinning Enhanced Visible and Infrared Imager (SEVIRI) is a payload onboard the second generation of the European stationary meteorological satellite (MSG). It has 12 channels, among which 3.92, 10.8, and 12.0 µm are suitable for SST retrieval [26,27]. In 2012, Le Borgne et al. verified 1-year SEVIRI SST with buoy SST, and the results showed the bias and STD of 0.07 °C and 0.38 °C, respectively [28]. Compared with the improved Argo data, SEVIRI SST showed a bias and an STD of <0.2 °C and <0.4 °C, respectively [29]. The Indian National Satellite-3D (INSAT-3D) imager is an improved version of the Very High-Resolution Radiometer (VHRR-2) onboard INSAT-3D, a new generation of stationary satellites in India. The bias between INSAT-3D imager SST and in situ, SST in the Indian Ocean was between −0.16 °C and −0.20 °C, and the bias between the two in the Arabian Ocean was −0.27 °C [30]. The weather imager (MI) is a payload onboard the Communication, Ocean, and Meteorological Satellite (COMS), Korea's first geostationary satellite and can retrieve SST. Woo et al. used multichannel SST (MCSST) and NLSST algorithms to retrieve SST. The results showed that for daytime, the MCSST algorithm had a bias and an RMSE of −0.05 °C and 0.65 °C, respectively, and the NLSST algorithm had a bias and an RMSE of −0.02 °C and 0.55 °C, respectively. For nighttime, the MCSST algorithm had a bias and an RMSE of −0.09 °C and 0.80 °C, respectively, and the NLSST algorithm had a bias and an RMSE of −0.11 °C and 0.71 °C, respectively [31].

Fengyun-2 (FY-2) is the first generation of the Chinese geostationary meteorological satellite series. VISSR is a payload onboard the FY-2C/D/E satellite. Infrared channels of 10.9 and 11.9 µm can be used for SST retrieval. When compared with MODIS/Terra data, FY-2C/D/E/VISSR SST, which was obtained by an atmospheric transmission model, MODTRAN showed a bias of  $-0.6 \pm 1.3$  °C,  $-0.2 \pm 1.5$  °C, and  $0.4 \pm 1.8$  °C, respectively [32]. Fengyun-4 (FY-4) is the second generation of the Chinese geostationary meteorological satellite series [33]. FY-4A is the first satellite of this series that was successfully launched on 17 December 2016, and finally located at 104.7°E, 36,500 km above the equator. FY-4A carries an advanced geosynchronous radiation imager (AGRI), interferometric atmospheric vertical sounding instrument, lightning imager, and space environment monitoring instrument. AGRI consists of 14 observation channels (three visible and near-infrared channels, three short-wave infrared channels, two medium-wave infrared channels, two water vapor channels, and four long-wave infrared channels). Channels with central wavelengths of 3.7, 10.7, and 12.0 µm can be used for SST retrieval, and the resulting high temporal resolution SST is greatly significant in studying air-sea interaction and coastal ocean modeling. The observation frequency of the full disk is 15 min, and the observation frequency of the Chinese region is 1 min. The spatial resolution ranges from 0.5 km to 1 km for visible channels and 2 km to 4 km for near-infrared and infrared channels [33–35]. The National Satellite Meteorology Center (NSMC) of the China Meteorological Administration (CMA) developed the FY-4A/AGRI SST product using the NLSST algorithm through the FY-4A/AGRI 10.7 and 12.0 µm channels [36]. FY-4A/AGRI SST showed an RMSE of 0.6961 °C in China seas from June 2018 to May 2019 compared with in situ data [37]. He et al. verified the 2019–2021 full disk FY-4A/AGRI SST with buoy SST. The results showed a bias and an

RMSE of  $-0.37^{\circ}\text{C}$  and  $0.98^{\circ}\text{C}$ , respectively, and a median and an RSD of  $-0.30^{\circ}\text{C}$  and  $0.90^{\circ}\text{C}$ , respectively [38]. Cui et al. verified full disk FY-4A/AGRI SST with in situ SST from July 2021 to June 2022. The results showed the optimum quality SST has a bias between  $-0.45^{\circ}\text{C}$  and  $-0.42^{\circ}\text{C}$  and an STD between  $0.81^{\circ}\text{C}$  and  $0.88^{\circ}\text{C}$  [36].

This paper aims to investigate the error sources of the AGRI SST products by comparing FY-4A/AGRI SST with the in situ SST and Himawari-8/AHI SST from January 2019 to December 2021. Section 2 introduces the materials and methods used in this study. Section 3 shows the results. Section 4 discusses the results. Finally, Section 5 presents the conclusion.

## 2. Materials and Methods

### 2.1. Materials

#### 2.1.1. FY-4A/AGRI Data

This study used FY-4A/AGRI level 1 GEO data, FY-4A/AGRI level 2 SST product, and FY-4A/AGRI level 2 atmospheric layer precipitable water (LPW) product from January 2019 to December 2021. The spatial resolution is 4 km, and the temporal resolution is 15 min. FY-4A/AGRI GEO contains 4-km positioning information obtained by FY-4A/AGRI L0 level source package data after geolocation processing. The data is stored in hierarchical data format (HDF) and contains datasets such as row number, column number, solar zenith angle, and satellite zenith angle, among others. By converting the lines and columns of FY-4A/AGRI data into latitude and longitude on the official website of the Fengyun satellite, the lines and columns in the geographical positioning data can also be converted into latitude and longitude. FY-4A AGRI operational SST products were retrieved using the NLSST algorithm [36]. The following is the regression equation of the AGRI SST algorithm.

$$\text{SST}_R = a_0 + a_1 \times T_{11} + a_2 \times T_{FG} \times (T_{11} - T_{12}) + a_3 \times (T_{11} - T_{12})(\sec\theta - 1) \quad (1)$$

$\text{SST}_R$  is the retrieved SST;  $T_{11}$  and  $T_{12}$  are the observed brightness temperature data of  $10.7\text{ }\mu\text{m}$  and  $12.0\text{ }\mu\text{m}$  channels,  $\theta$  is the satellite zenith angle, and  $T_{FG}$  is the first guess SST and  $a_i$  ( $i = 0, 1, 2, 3$ ) the regression coefficients of SST were calculated by regression between in situ SST and the temperature observed by AGRI. AGRI SST data were quality controlled according to the satellite zenith angle, spatial consistency in  $3 \times 3^{\circ}$  data square and comparison with the background SST. There are four quality flags. The quality level 0 represents good, 1 represents suboptimal, 2 represents bad, and 3 represents invalid. Only the observations with a zenith angle of less than  $70^{\circ}$  were retrieved. The number of clear sky ocean pixels was calculated in each  $3 \times 3^{\circ}$  square. The retrieved SST was compared with the background SST. When the pixels met the climatological threshold against the background SST and all the pixels in the  $3 \times 3^{\circ}$  square were clear sky ocean pixels, the data quality level was 0. When the pixels only met the climatological threshold test, the quality level was 1, and for other cases, the quality level was 2 [36]. The data is stored in network common data form (NetCDF) and contains datasets such as SST and data quality, among others. This study used the data of high-accuracy applications with level 0 quality. FY-4A/AGRI LPW is an atmospheric layer precipitable water product of FY-4A/AGRI [39]. The data is stored in NetCDF4 and contains datasets such as total precipitable water and low, middle, and high levels of precipitable water, among others [39]. The data can be downloaded by ftp at [nsmc.org.cn](http://nsmc.org.cn) (accessed on 30 April 2023).

#### 2.1.2. Himawari-8/AHI Data

Himawari-8 [16] AHI has 16 observation channels (three visible channels, three near-infrared channels, and ten infrared channels), and channels with central wavelengths of  $3.9$ ,  $8.6$ ,  $10.4$ ,  $11.2$ , and  $12.4\text{ }\mu\text{m}$  are used for SST retrieval. The observation frequency of the full disk is 10 min, and that of the Japanese region is 2.5 min. The spatial resolution of Himawari-8/AHI is  $0.5\text{--}1\text{ km}$  for visible bands and  $1\text{--}2\text{ km}$  for near-infrared and infrared bands. Himawari-8/AHI SST product was developed by JAXA using a quasi-physical



algorithm [17], the level 2 data were used. The data is stored in NetCDF, and the data version is 2.0. The projection mode is equal-angle projection, the spatial resolution is  $0.02^\circ$ , the time resolution is 10 min, and the data includes datasets, such as SST, longitude, latitude, data quality, solar zenith angle, and satellite zenith angle. This study used the data of high-accuracy applications with level 5 quality from January 2019 to December 2021. The data can be downloaded by ftp at <https://www.eorc.jaxa.jp/ptree/> (accessed on 30 April 2023).

### 2.1.3. In Situ SST

The in situ SST quality monitor (iQuam) version 2.10 dataset was developed at the NOAA Center for Satellite Application and Research (STAR). The historical data is organized and stored into files by month, and the data file is in an HDF format. Datasets include SST, data quality, latitude, longitude, time, depth, atmospheric temperature, and atmospheric pressure. The three main functions of iQuam SST are quality control of SST, near real-time online monitoring of SST, and providing reformatted SST data [40]. Considering the accuracy of in situ measurements, the buoy data of the highest quality, level 5 quality, from January 2019 to December 2021 were used in this study. The data can be downloaded by ftp at <https://www.star.nesdis.noaa.gov/socd/sst/iquam/> (accessed on 30 April 2023).

## 2.2. Method

### 2.2.1. Study Area

Figure 1 shows the spatial coverage of the full-disk region of FY-4A/AGRI and Himawari-8/AHI. The blue and red areas represent FY-4A/AGRI and Himawari-8/AHI, respectively. Figure 2 shows the distribution of FY-4A/AGRI SST and Himawari-8/AHI SST products on 1 January 2020, respectively, while the color represents the temperature. This paper selects the overlap area between Himawari-8/AHI and FY-4A/AGRI as the study area.

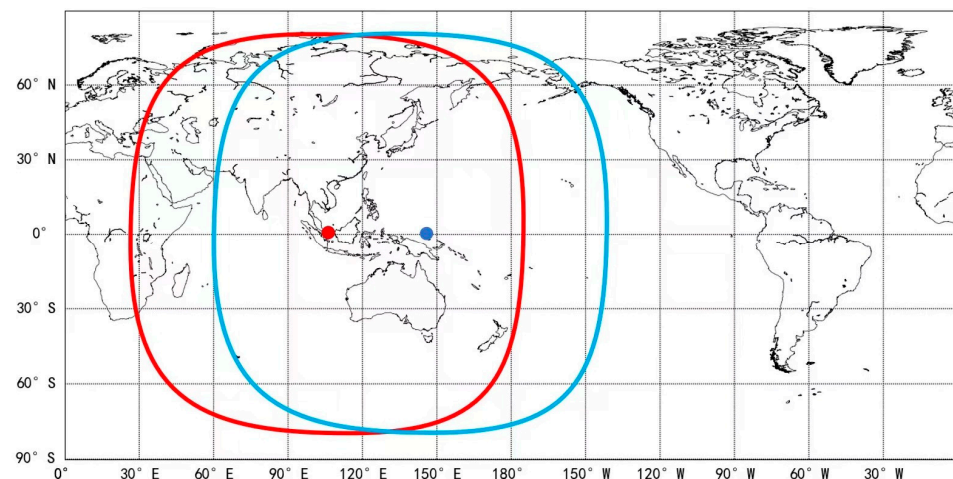


**Figure 1.** Spatial coverage of the full-disk region of FY-4A/AGRI (red) and Himawari-8/AHI (blue).

### 2.2.2. Matching Method

AGRI's spatial and temporal resolution is 4 km and 15 min [33], and AHI's spatial and temporal resolution is  $0.02^\circ$  and 10 min, respectively. Since the spatial and temporal resolutions of the two data sets were different, the matching criteria of the temporal window was 30 min, and the spatial window was  $0.1^\circ$ . The highest-quality data were then selected. The statistics for daytime were calculated from data where the solar zenith angle was  $\leq 85^\circ$ , while the statistics for nighttime were calculated from the data where the solar zenith angle was  $> 85^\circ$ . The data agreeing within 30 min was projected into a grid of  $0.1^\circ \times 0.1^\circ$  according to the latitude and longitude of the observations, and the SST of each data

source was averaged in each grid. The matchups were produced only when all 3 SST data were available.

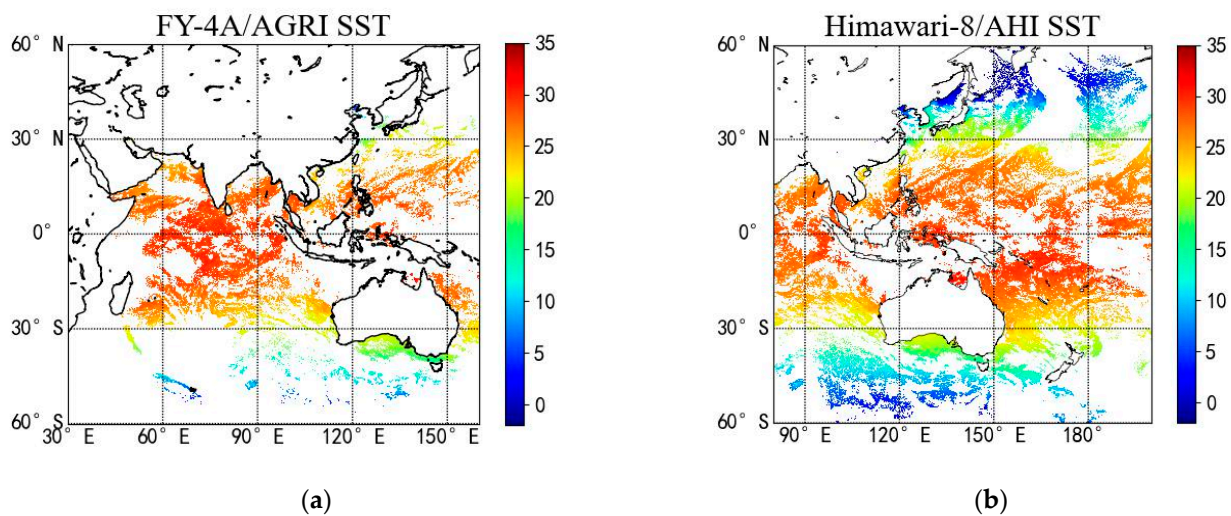


**Figure 2.** Satellite SST on 1 January 2020. (a) FY-4A/AGRI SST; (b) Himawari-8/AHI SST.

The SST after data projection was the mean SST observed in the  $0.1^\circ \times 0.1^\circ$  grid. The matchup data were further screened considering the inhomogeneity of the data within one grid since the spatial resolution was different. The difference between the minimum and maximum SST of FY-4A/AGRI SST and Himawari-8/AHI SST located in the same grid was calculated. The matchups in which the difference between the minimum and maximum SST was greater than  $1^\circ\text{C}$  were removed to remove the influence of SST fronts on the results. Since many points fell into a grid during the Himawari-8 projection, matchups with fewer than 70 Himawari-8/AHI points in a grid were removed to reduce random errors and ensure clear sky matchups. Finally, the matching results after the removal of outliers were obtained.

### 3. Results

The statistics were derived from the matchup data. Here, the number (N), bias, median, standard deviation (STD), robust standard deviation (RSD), and root mean square error (RMSE) of the matchups were calculated. Table 1 presents the statistics of the SST difference in the matchups for daytime and nighttime from January 2019 to December 2021.

**Table 1.** Statistics of the differences between various SST estimates in the matchups for daytime and nighttime from January 2019 to December 2021.

	N	Bias (°C)	Median (°C)	STD (°C)	RSD (°C)	RMSE (°C)
Daytime						
AGRI SST-Buoy SST	176,178	−0.12	−0.05	0.76	0.68	0.77
AHI SST-Buoy SST		−0.15	−0.13	0.58	0.44	0.61
AGRI SST-AHI SST		0.04	0.10	0.78	0.70	0.78
Nighttime						
AGRI SST-Buoy SST	150,152	−0.00	0.05	0.78	0.72	0.78
AHI SST-Buoy SST		−0.30	−0.25	0.60	0.45	0.67
AGRI SST-AHI SST		0.30	0.34	0.81	0.76	0.86

As presented in Table 1, the total number of all matchups was 176,178 and 150,152 for daytime and nighttime, respectively. The STD, RSD and RMSE of FY-4A/AGRI SST were higher than those of Himawari-8/AHI SST for both daytime and nighttime. The statistics

shown in Table 1 were better than those obtained by He et al. [38] and Cui et al. [36]. The bias of AGRI SST minus in situ SST in this study was close to 0 °C, and STD, RSD, and RMSE were also lower than He et al. and Cui et al. The quality controls in the matching procedure to remove the influence of an inhomogeneous SST field, and the selections of the most clear-sky data in the spatial window led to more accurate matchups between satellite and in situ data. Figure 3 shows the density scatterplots of matchups for daytime and nighttime from January 2019 to December 2021. The correlation coefficients between AGRI SST and in situ SST exceeded 0.991 for both daytime and nighttime, which exceeded 0.990 between AGRI SST and AHI SST for both daytime and nighttime, reaching the significance level of 0.001. Figure 4 shows the relative frequencies of each difference. The red lines show the Gaussian distributions defined using the mean and STD of the difference between different observation types. The histogram of AGRI minus buoy SST difference shows a slight cold tail for daytime which may be caused by some undetected clouds. AHI SST minus in situ SST shows a more negative bias for nighttime, consistent with the results in Table 1. FY-4A/AGRI SST is higher than Himawari-8/AHI SST for nighttime.

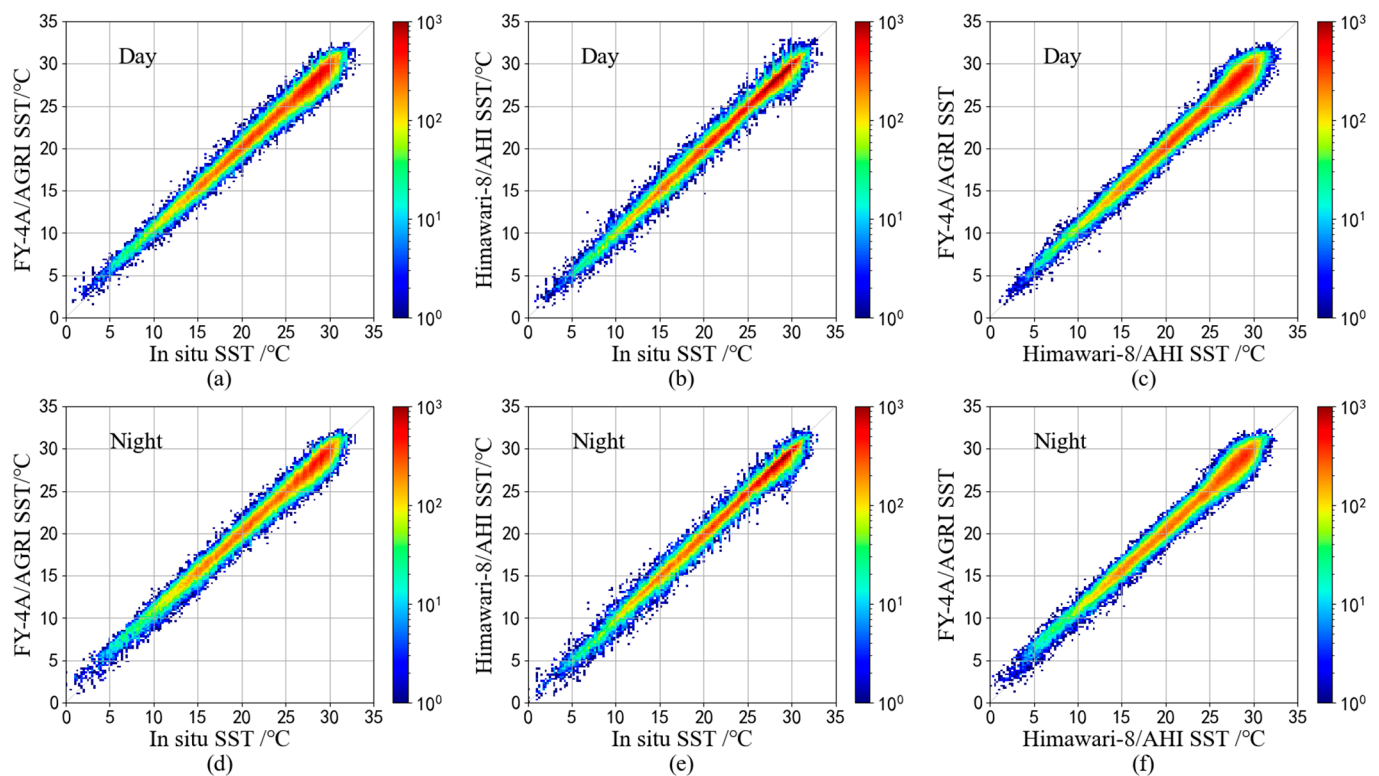


**Figure 3.** Density scatterplots of matchups for daytime and nighttime from January 2019 to December 2021. (a) and (d) FY-4A/AGRI SST minus in situ SST; (b) and (e) Himawari-8/AHI SST minus in situ SST; (c) and (f) FY-4A/AGRI SST minus Himawari-8/AHI SST.

The SST matchups were divided by month to observe the change in SST accuracy over time. Figure 5a–c shows the monthly variation of SST bias and STD. The red line, blue line, and vertical error bar represent the monthly bias for daytime, the monthly bias for nighttime, and the monthly STD, respectively.

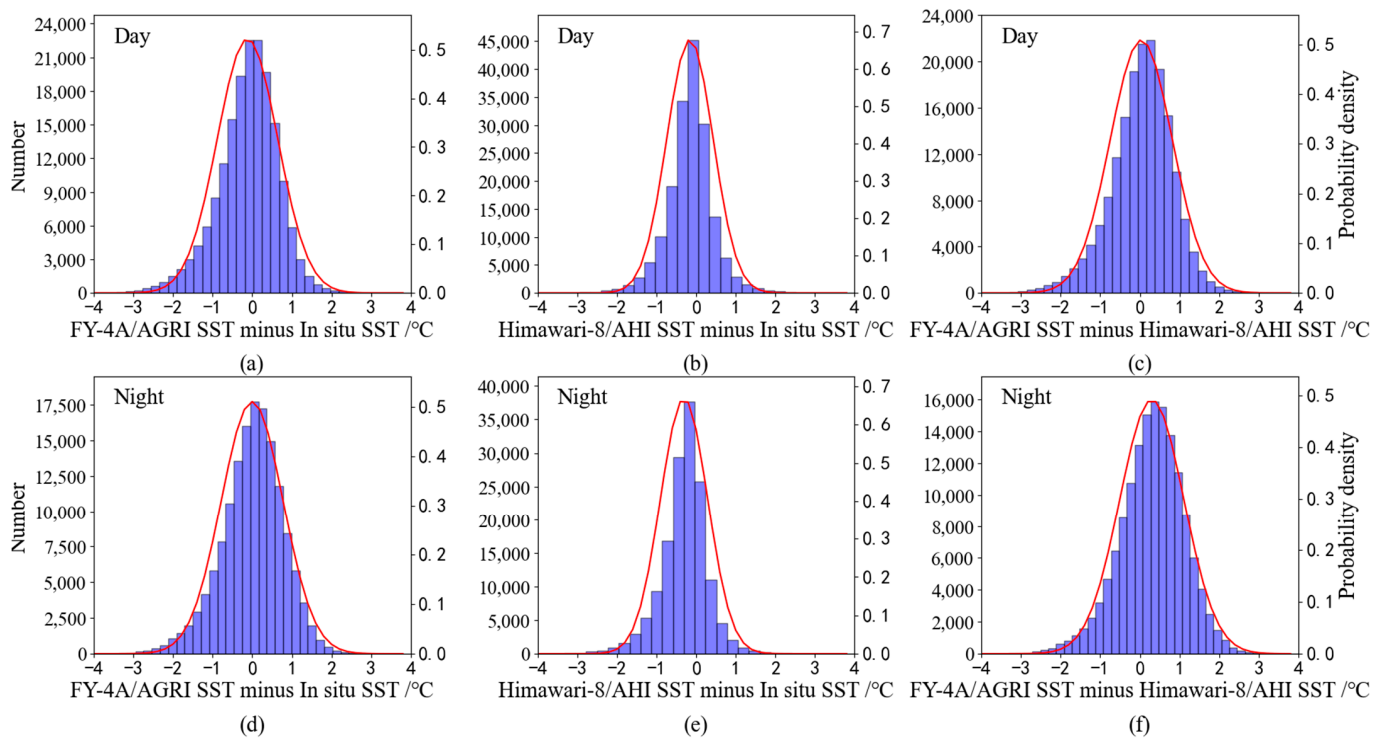


**Figure 4.** Histograms and statistics of matchups for daytime and nighttime from January 2019 to December 2021. (a) and (d) FY-4A/AGRI SST minus in situ SST; (b) and (e) Himawari-8/AHI SST minus in situ SST; (c) and (f) FY-4A/AGRI SST minus Himawari-8/AHI SST.

As shown in Figure 5a, the bias and STD of FY-4A/AGRI SST showed no seasonal correlation. But the bias of FY-4A/AGRI SST had an obvious bias jump in the study period. The bias increased significantly in the six months after August 2020, which may be related to the operational calibration update of FY-4A/AGRI in August 2020 [41]. The calibration update affected the brightness temperature of satellite data, but the SST retrieval coefficients had not been updated. Therefore, a relatively larger error was caused after the calibration update. As shown in Figure 5b, Himawari-8/AHI SST exhibited a larger negative bias for nighttime during the study period. It may be due to a failure to detect clouds because of the absence of visible data [17].

A three-way error analysis, a method to empirically estimate the errors of different data observation types, was used to estimate the errors of AGRI, AHI and buoy SST for daytime and nighttime from January 2019 to December 2021, Equation (2) can be used [42–44].

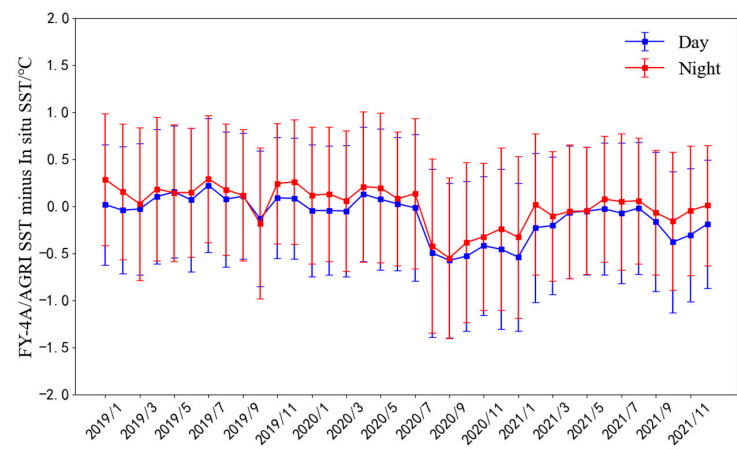
$$\begin{aligned}\sigma_1 &= \left[ \frac{1}{2}(V_{12} + V_{31} - V_{23}) \right]^{1/2} \\ \sigma_2 &= \left[ \frac{1}{2}(V_{23} + V_{12} - V_{31}) \right]^{1/2} \\ \sigma_3 &= \left[ \frac{1}{2}(V_{31} + V_{23} - V_{12}) \right]^{1/2}\end{aligned}\quad (2)$$

where  $\sigma_i$  is the error of different observation type  $i$  (where  $i = 1, 2$ , or  $3$ ),  $V_{ij}$  is the variance of the difference between observation types  $i$  and  $j$ .

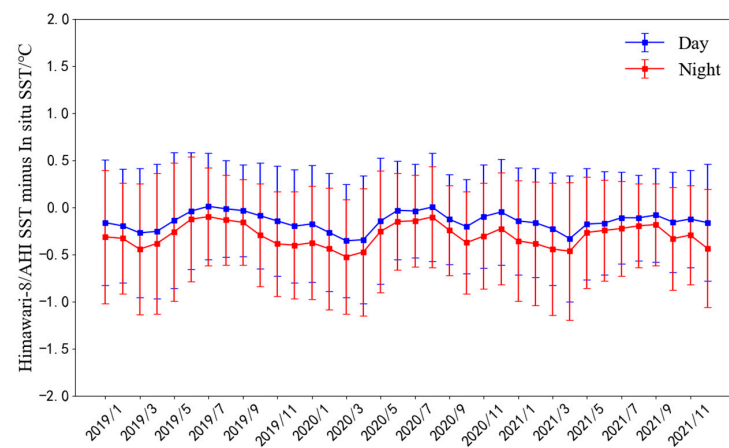
As shown in Table 2, the three years estimated SST errors for AGRI, AHI, and buoy SST were 0.65, 0.43, and 0.39 °C for daytime and 0.67, 0.45, and 0.39 °C for nighttime. It indicated that the accuracy of AHI and in situ was better than AGRI. Table 2 showed some discrepancies compared with He et al. [38], which conducted a three-way analysis using AGRI SST, in situ SST data and 1/4° daily optimum interpolation SST data. The error of AGRI SST was 0.83 °C in He et al., and it was 0.65 °C for daytime and 0.67 °C for nighttime in this study. The differences may be caused by the quality controls in matchups and the



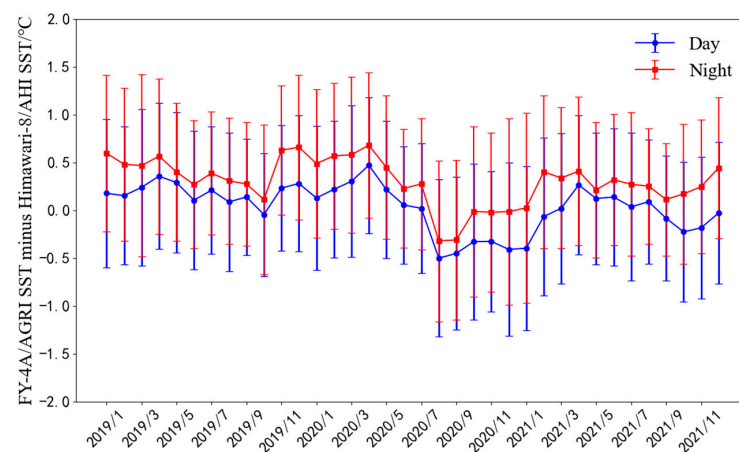
usage of different in situ measurement platforms. In situ data from ship measurements were not used in our study, which had a lower accuracy [43].



(a)



(b)



(c)

**Figure 5.** (a). Bias and STD between FY-4A/AGRI SST and in situ SST over time; (b) bias and STD between Himawari-8/AHI SST and in situ SST over time; and (c) Bias and STD between FY-4A/AGRI SST and Himawari-8/AHI SST over time.

**Table 2.** Estimated AGRI, AHI and buoy SST errors using three-way analysis for daytime and nighttime from January 2019 to December 2021.

$\sigma$ (°C)								
Daytime					Nighttime			
year	2019	2020	2021	2019–2021	2019	2020	2021	2019–2021
AGRI	0.55	0.71	0.64	0.65	0.59	0.75	0.61	0.67
AHI	0.45	0.44	0.42	0.43	0.46	0.44	0.45	0.45
Buoy	0.41	0.39	0.38	0.39	0.39	0.39	0.39	0.39

#### 4. Discussion

This section discussed the spatial distribution of SST bias and the relationship between FY-4A/AGRI SST accuracy and satellite zenith angle and water vapor to further analyze the factors influencing SST accuracy.

##### 4.1. Spatial Distribution of SST Bias

We first investigated the spatial distribution of SST bias. Figures 6 and 7 show the spatial relationship between the bias, STD, and number of matchups in the  $2^\circ \times 2^\circ$  grid for daytime and nighttime from January 2019 to December 2021. Compared with the in situ SST, a negative bias was observed in the middle and low latitudes of FY-4A/AGRI SST, and a positive bias was observed in the high latitudes of the southern hemisphere. This distribution may be related to one set of coefficients used in the retrieval algorithm of full-disk AGRI SST [36]. In addition, more negative bias appears near  $160^\circ\text{E}$  because the Pacific region near  $160^\circ\text{E}$  is at the edge of the AGRI SST. NLSST uses a multi-channel atmospheric correction to estimate SST, but it may still have relatively large errors due to high water vapor. As shown in Figures 6c and 7c, though the matchups almost covered the entire area where the two satellites overlapped, the spatial density distribution of matchups was not uniform because the distribution of in situ data was not uniform. The SST algorithm had lower accuracy in the area with less in situ data. This affected the distribution of error statistics to a certain extent. The larger AGRI errors may result from the combined influence of high satellite zenith angle, water vapor, not uniform in situ data distribution and clouds. Himawari-8/AHI SST showed more negative bias near the equator, and  $80^\circ\text{E}$  longitude, a failure to detect clouds may contribute to these biases [17].

##### 4.2. Relationship between SST Accuracy and Satellite Zenith Angle

The relationship between FY-4A/AGRI SST error and satellite zenith angle was investigated. According to the satellite zenith angle, the matchups were divided into seven segments, which were  $0\text{--}10^\circ$ ,  $10\text{--}20^\circ$ ,  $20\text{--}30^\circ$ ,  $30\text{--}40^\circ$ ,  $40\text{--}50^\circ$ ,  $50\text{--}60^\circ$ ,  $60\text{--}70^\circ$ , respectively. The bias, STD, and numbers of FY-4A/AGRI SST minus in situ SST of each segment were calculated respectively. Figure 8 shows the relationship between FY-4A/AGRI SST accuracy and satellite zenith angle. When the satellite zenith angle was larger than  $50^\circ$ , the bias and STD could reach  $-0.54^\circ\text{C}$  and  $0.96^\circ\text{C}$ , respectively, during daytime, and the bias and STD could reach  $-0.35^\circ\text{C}$  and  $0.93^\circ\text{C}$ , respectively, during nighttime. It can be seen that when the zenith angle of the satellite was larger than  $50^\circ$ , the accuracy of FY-4A/AGRI SST was affected for both daytime and nighttime. This is mainly because, with the increase of the zenith angle of the satellite, the radiation needs to pass through a longer distance to the satellite, making the radiation more susceptible to atmospheric absorption and scattering in the transmission process.

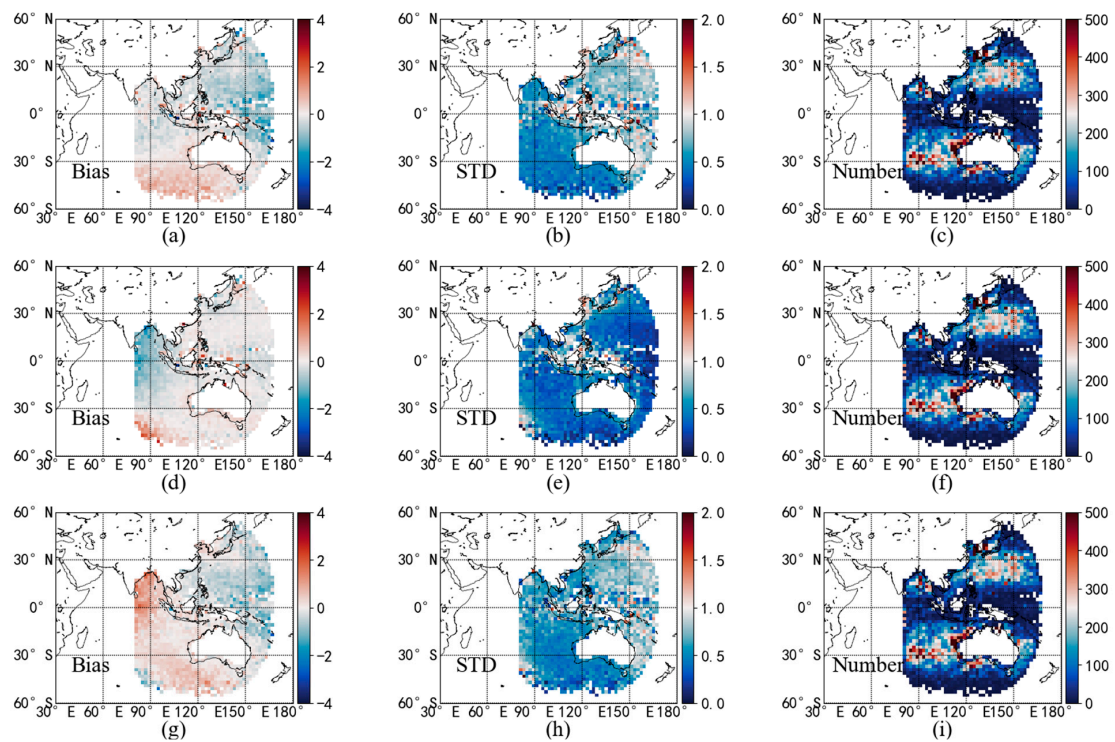


**Figure 6.** Bias, STD, and number of matchups calculated for each  $2^\circ \times 2^\circ$  square for daytime from January 2019 to December 2021. (a–c) FY-4A/AGRI SST minus in situ SST. (d–f) Himawari-8/AHI SST minus in situ SST. (g–i) FY-4A/AGRI SST minus Himawari-8/AHI SST.

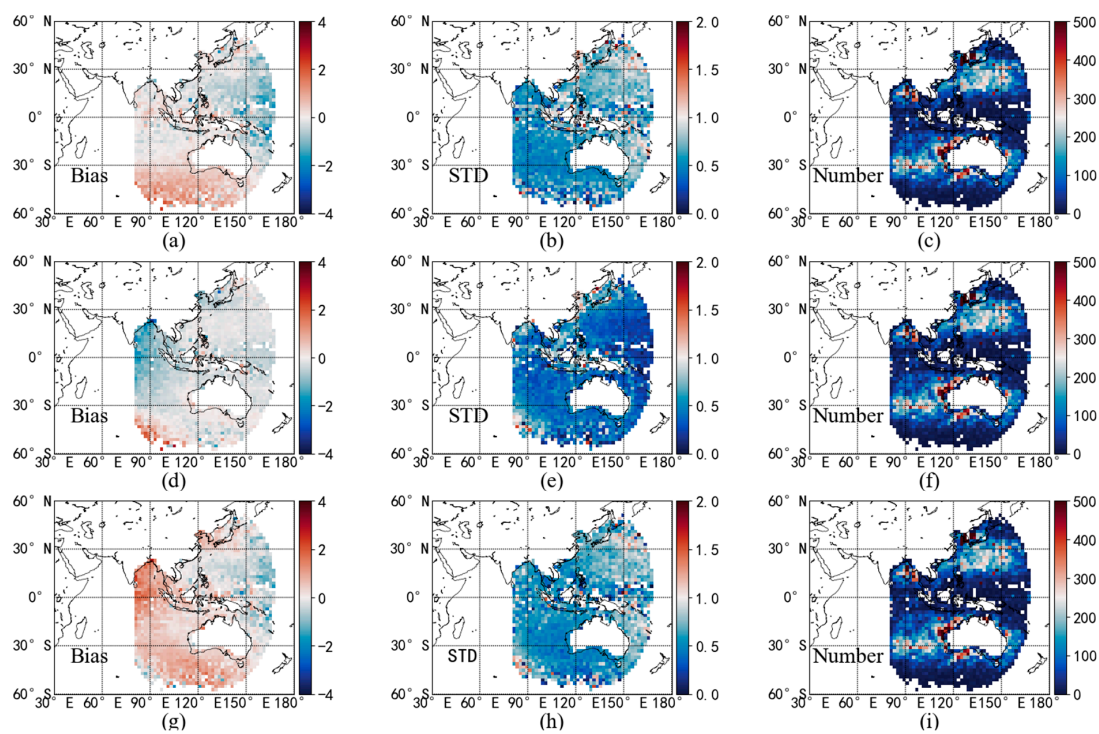


**Figure 7.** Bias, STD, and number of matchups calculated for each  $2^\circ \times 2^\circ$  square for nighttime from January 2019 to December 2021. (a–c) FY-4A/AGRI SST minus in situ SST. (d–f) Himawari-8/AHI SST minus in situ SST. (g–i) FY-4A/AGRI SST minus Himawari-8/AHI SST.

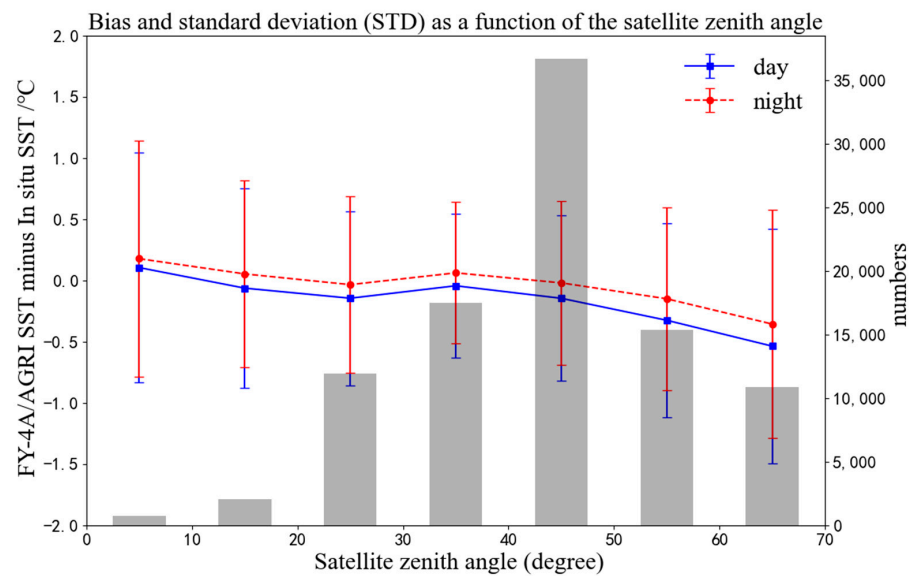


**Figure 8.** Relationship between FY-4A/AGRI SST accuracy and satellite zenith angle.

#### 4.3. Relationship between SST Accuracy and Water Vapor

According to the water vapor content, the matchups were divided into seven segments, which were 0–1 g/kg, 1–2 g/kg, 2–3 g/kg, 3–4 g/kg, 4–5 g/kg, 5–6 g/kg, 6–7 g/kg, respectively. The bias, STD, and numbers of FY-4A/AGRI SST minus in situ SST of each segment were calculated, respectively. Figure 9 shows the relationship between FY-4A/AGRI SST accuracy and water vapor. The red line, blue line, and vertical error bar represented the bias for daytime, the bias for nighttime, and the STD, respectively. The black histogram represented the number of matchups. When the water vapor was more than 6 g/kg, the bias and STD can reach  $-0.54^{\circ}\text{C}$  and  $0.96^{\circ}\text{C}$ , respectively, for daytime, and the STD can reach  $0.94^{\circ}\text{C}$  for nighttime. It can be seen that STD increased as the water vapor increased, and water vapor can affect the accuracy of FY-4A/AGRI SST. Since the cloud coverage was relatively higher in regions with high water vapor, the number of satellite SST was reduced in the regions. The less number of matchups was one factor contributing to the lower accuracy of the SST algorithm in the regions with high water vapor.

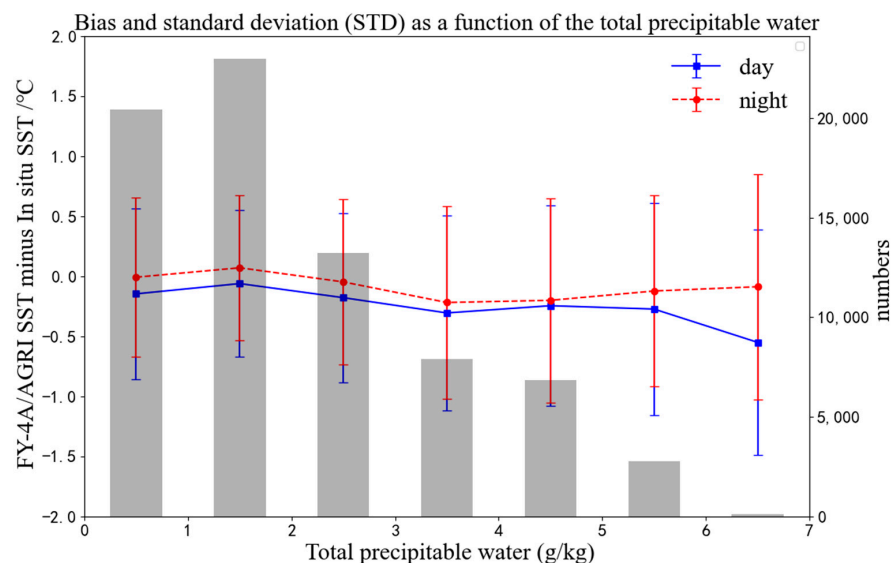


**Figure 9.** Relationship between FY-4A/AGRI SST accuracy and water vapor.



In the future, we will divide the water vapor intervals according to the brightness temperature difference of FY-4A/AGRI 10.7 and 12.0  $\mu\text{m}$  channels and develop an SST algorithm with different retrieval coefficients according to water vapor range.

## 5. Conclusions

This paper mainly investigated the error sources of the AGRI SST products by comparing FY-4A/AGRI SST with in situ SST and Himawari-8/AHI SST with the time series from January 2019 to December 2021. The following are the main conclusions of this study:

Compared with in situ SST, FY-4A/AGRI SST had a bias of  $-0.12\text{ }^{\circ}\text{C}$ , and the median was  $-0.05\text{ }^{\circ}\text{C}$ . STD was  $0.76\text{ }^{\circ}\text{C}$ , RSD and RMSE were  $0.68\text{ }^{\circ}\text{C}$  and  $0.77\text{ }^{\circ}\text{C}$ , respectively, for daytime, and the bias was  $0.00\text{ }^{\circ}\text{C}$ , the median was  $0.05\text{ }^{\circ}\text{C}$ , STD was  $0.78\text{ }^{\circ}\text{C}$ , RSD and RMSE were  $0.72\text{ }^{\circ}\text{C}$  and  $0.78\text{ }^{\circ}\text{C}$ , respectively, for nighttime. The results of the difference between FY-4A/AGRI SST and Himawari-8/AHI SST showed a bias of  $0.04\text{ }^{\circ}\text{C}$ , median of  $0.10\text{ }^{\circ}\text{C}$ , STD of  $0.78\text{ }^{\circ}\text{C}$ , RSD of  $0.70\text{ }^{\circ}\text{C}$ , and RMSE of  $0.78\text{ }^{\circ}\text{C}$  for daytime and the bias of  $0.30\text{ }^{\circ}\text{C}$ , median of  $0.34\text{ }^{\circ}\text{C}$ , STD of  $0.81\text{ }^{\circ}\text{C}$ , RSD of  $0.76\text{ }^{\circ}\text{C}$ , and RMSE of  $0.86\text{ }^{\circ}\text{C}$  for nighttime.

The STD, RSD and RMSE of FY-4A/AGRI SST were higher than those of Himawari-8/AHI SST for both daytime and nighttime. One set of coefficients was used in the retrieval algorithm of full-disk AGRI SST, which may lead to larger errors of AGRI than AHI SST. It can be seen that FY-4A/AGRI SST accuracy needs to be improved. During the study period, no significant correlation was found between the bias and STD of FY-4A/AGRI SST difference and time, but there was an obvious bias jump in the study period may be because of the operation calibration update.

The AGRI SST accuracy is dependent on the satellite zenith angle and water vapor. Further research on the FY-4A/AGRI SST retrieval algorithm accounting for the variability of water vapor will be conducted to improve the FY-4A/AGRI SST accuracy.

**Author Contributions:** Conceptualization, C.Y. and L.G.; methodology, C.Y. and L.G.; data processing, C.Y.; formal analysis, C.Y., L.G. and X.S.; writing—original draft preparation, C.Y.; writing—review and editing, L.G.; funding acquisition, L.G. All authors have read and agreed to the published version of the manuscript.

**Funding:** The research was supported by the Hainan Provincial Natural Science Foundation of China (No.122CXTD519) and the National Key R&D Program of China (No.2022YFC3104900/2022YFC3104905).

**Data Availability Statement:** FY-4A/AGRI data were obtained at <http://satellite.nsmc.org.cn/> (accessed on 30 April 2023). Himawari-8/AHI data were downloaded at <https://www.eorc.jaxa.jp/ptree/> (accessed on 30 April 2023). The iQuam data were downloaded at <https://www.star.nesdis.noaa.gov/socd/sst/iquam/> (accessed on 30 April 2023).

**Acknowledgments:** FY-4A/AGRI data were provided by the National Satellite Meteorological Center. Himawari-8/AHI data were provided by Japan Meteorological Agency. iQuam data were developed at NOAA Center for Satellite Application and Research (STAR).

**Conflicts of Interest:** The authors declare no conflict of interest. The funders had no role in the study's design; in the collection, analyses, or interpretation of data; in the writing of the manuscript, or in the decision to publish the results.

## References

1. Wanninkhof, R.; Asher, W.E.; Ho, D.T.; Sweeney, C.; McGillis, W.R. Advances in quantifying air-sea gas exchange and environmental forcing. *Ann. Rev. Mar. Sci.* **2009**, *1*, 213–244. [CrossRef]
2. Tandeo, P.; Chapron, B.; Ba, S.; Autret, E.; Fablet, R. Segmentation of mesoscale ocean surface dynamics using satellite SST and SSH observations. *IEEE Trans. Geosci. Remote Sens.* **2014**, *52*, 4227–4235. [CrossRef]
3. Martin, S. *An Introduction to Ocean Remote Sensing*, 2nd ed.; Cambridge University Press: Cambridge, UK, 2014; pp. 219–241.
4. Maul, G.A. Application of GOES visible-infrared data to quantifying mesoscale ocean surface temperatures. *J. Geophys. Res.* **1981**, *86*, 8007–8021. [CrossRef]

5. Bates, J.J.; Smith, W.L. Sea surface temperature: Observations from geostationary satellites. *J. Geophys. Res.* **1985**, *90*, 11609. [CrossRef]
6. Minnett, P.J.; Álvarez-Azcárate, A.; Chin, T.M.; Corlett, G.K.; Gentemann, C.L.; Karagali, I.; Li, X.; Marsouin, A.; Marullo, S.; Maturi, E.; et al. Half a century of satellite remote sensing of sea-surface temperature. *Remote Sens. Environ.* **2019**, *233*, 111366. [CrossRef]
7. Maturi, E.; Harris, A.; Merchant, C.; Mittaz, J.; Potash, B.; Meng, W.; Sapper, J. NOAA's sea surface temperature products from operational geostationary satellites. *Bull. Am. Meteorol. Soc.* **2008**, *89*, 1877–1888. [CrossRef]
8. Merchant, C.J.; Harris, A.R.; Maturi, E.; Embury, O.; MacCallum, S.N.; Mittaz, J.; Old, C.P. Sea Surface Temperature Estimation from the Geostationary Operational Environmental Satellite-12 (GOES-12). *J. Atmos. Oceanic Technol.* **2009**, *26*, 570–581. [CrossRef]
9. Azevedo, M.H.; Rudorff, N.; Aravéquia, J.A. Evaluation of the ABI/GOES-16 SST Product in the Tropical and Southwestern Atlantic Ocean. *Remote Sens.* **2021**, *13*, 192. [CrossRef]
10. Ignatov, A. GOES-R Advanced Baseline Imager (ABI) Algorithm Theoretical Basis Document for Sea Surface Temperature. NOAA NESDIS Center for Satellite Applications and Research. 2010. Available online: [https://www.star.nesdis.noaa.gov/goesr/documents/ATBDs/Baseline/ATBD\\_GOES-R\\_SST-v2.0\\_Aug2010.pdf](https://www.star.nesdis.noaa.gov/goesr/documents/ATBDs/Baseline/ATBD_GOES-R_SST-v2.0_Aug2010.pdf) (accessed on 20 August 2023).
11. Petrenko, B.; Ignatov, A.; Kihai, Y.; Dash, P. Sensor-specific error statistics for SST in the advanced clear-sky processor for oceans. *J. Atmos. Ocean. Technol.* **2016**, *33*, 345–359. [CrossRef]
12. Luo, B.; Minnett, P.J. Skin sea surface temperatures from the GOES-16 ABI validated with those of the shipborne M-AERI. *IEEE Trans. Geosci. Remote Sens.* **2021**, *59*, 9902–9913. [CrossRef]
13. Tanahashi, S.; Kawamura, H.; Matsuura, T.; Takajashi, T.; Yusa, H. Improved estimates of wide-ranging sea surface temperature from GMS S-VISSR data. *J. Oceanogr.* **2000**, *56*, 345–358. [CrossRef]
14. Kawamura, H.; Qin, H.; Sakaida, F.; Setiawan, R.Y. Hourly sea surface temperature retrieval using the Japanese geostationary satellite, multi-functional transport satellite (MTSAT). *J. Oceanogr.* **2010**, *66*, 61–70. [CrossRef]
15. Ditri, A.; Minnett, P.; Liu, Y.; Kilpatrick, K.; Kumar, A. The accuracies of Himawari-8 and MTSAT-2 sea-surface temperatures in the tropical Western Pacific Ocean. *Remote Sens.* **2018**, *10*, 212. [CrossRef]
16. Bessho, K.; Date, K.; Hayashi, M.; Ikeda, A.; Imai, T.; Inoue, H.; Kumagai, Y.; Miyakawa, T.; Murata, H.; Ohno, T.; et al. An introduction to Himawari-8/9—Japan's new-generation geostationary meteorological satellites. *J. Meteorol. Soc. Jpn.* **2016**, *94*, 151–183. [CrossRef]
17. Kurihara, Y.; Murakami, H.; Kachi, M. Sea surface temperature from the new Japanese geostationary meteorological Himawari-8 satellite. *Geophys. Res. Lett.* **2016**, *43*, 1234–1240. [CrossRef]
18. Kramar, M.; Ignatov, A.; Petrenko, B.; Kihai, Y.; Dash, P. Near Real Time SST Retrievals from Himawari-8 at NOAA Using ACSPO System. In Proceedings of the Ocean Sensing and Monitoring VIII SPIE, Baltimore, MD, USA, 17–21 April 2016; Available online: [https://www.star.nesdis.noaa.gov/pub/sod/osb/mkramar/paper\\_SPIE16/07/SPIE\\_Proc\\_9827-21\\_Kramar.pdf](https://www.star.nesdis.noaa.gov/pub/sod/osb/mkramar/paper_SPIE16/07/SPIE_Proc_9827-21_Kramar.pdf) (accessed on 20 August 2023).
19. Beggs, H. Ch 14: Temperature. In *Earth Observation: Data Processing and Applications*; Harrison, B.A., Anstee, J.A., Dekker, A., Phinn, S., Mueller, N., Byrne, G., Eds.; CRCSP: Melbourne, Australia, 2020; Volume 3B, Applications—Surface Waters; pp. 245–279.
20. Kusuma, D.W.; Murdimanto, A.; Aden, L.Y.; Sukresno, B.; Jatisworo, D.; Hanintyo, R. Sea surface temperature dynamics in Indonesia. *IOP Conf. Ser. Earth Environ. Sci.* **2017**, *98*, 012038. [CrossRef]
21. Sukresno, B.; Hanintyo, R.; Kusuma, D.W.; Jatisworo, D.; Murdimanto, A. Three-way error analysis of sea surface temperature (SST) between Himawari-8, buoy, and MUR SST in Savu Sea. *Int. J. Remote Sens. Earth Sci.* **2018**, *15*, 25. [CrossRef]
22. Yang, M.L.; Guan, L.; Beggs, H.; Morgan, N.; Kurihara, Y.; Kachi, M. Comparison of Himawari-8 AHI SST with shipboard skin SST measurements in the Australian region. *Remote Sens.* **2020**, *12*, 1237. [CrossRef]
23. Tu, Q.; Hao, Z. Validation of sea surface temperature derived from Himawari-8 by JAXA. *IEEE J. Sel. Top. Appl. Earth Obs. Remote Sens.* **2020**, *13*, 448–459. [CrossRef]
24. Wang, P.; Zhu Ge, X.Y.; Chen, B.J.; Lu, Y.L.; Xiao, Y.X.; Xia, F. Retrieval of sea surface temperature in all sky conditions based on AHI observations. *J. Meteorol. Sci.* **2020**, *40*, 249–256. (In Chinese)
25. Hsu, P.C. Evaluation of wind and solar insolation influence on ocean near-surface temperature from in situ observations and the geostationary Himawari-8 satellite. *Remote Sens.* **2022**, *14*, 4975. [CrossRef]
26. Aminou, D. MSG's SEVIRI Instrument. *ESA Bull.* **2002**, *111*, 15–17.
27. Schmid, J. The SEVIRI Instrument. In Proceedings of the 2000 EUMETSAT Meteorological Satellite Data User's Conference, Bologna, Italy, 29 May–2 June 2000; Available online: [https://www-cdn.eumetsat.int/files/2020-04/pdf\\_ten\\_msg\\_seviri\\_instrument.pdf](https://www-cdn.eumetsat.int/files/2020-04/pdf_ten_msg_seviri_instrument.pdf) (accessed on 20 August 2023).
28. Le Borgne, P.; Legendre, G.; Péré, S. Comparison of MSG/SEVIRI and drifting buoy derived diurnal warming estimates. *Remote Sens. Environ.* **2012**, *124*, 622–626. [CrossRef]
29. Castro, S.L.; Wick, G.A.; Buck, J.J.H. Comparison of diurnal warming estimates from unpumped Argo data and SEVIRI satellite observations. *Remote Sens. Environ.* **2014**, *140*, 789–799. [CrossRef]
30. Tyagi, G.; Babu, K.N.; Mathur, A.K.; Solanki, H.A. INSAT-3D and MODIS retrieved sea surface temperature validation and assessment over waters surrounding the Indian subcontinent. *Int. J. Remote Sens.* **2018**, *39*, 1575–1592. [CrossRef]
31. Woo, H.J.; Park, K.A.; Li, X.; Lee, E.Y. Sea surface temperature retrieval from the first Korean geostationary satellite COMS data: Validation and error assessment. *Remote Sens.* **2018**, *10*, 1916. [CrossRef]

32. Jiang, G.; Liu, R. Retrieval of sea and land surface temperature from SVISSR/FY-2C/D/E measurements. *IEEE Trans. Geosci. Remote Sens.* **2014**, *52*, 6132–6140. [[CrossRef](#)]
33. Yang, J.; Zhang, Z.; Wei, C.; Lu, F.; Guo, Q. Introducing the new generation of Chinese geostationary weather satellites, Fengyun-4. *Bull. Am. Meteorol. Soc.* **2017**, *98*, 1637–1658. [[CrossRef](#)]
34. Zhang, P.; Guo, Q.; Chen, B.Y.; Feng, X. The Chinese next-generation geostationary meteorological satellite FY-4 compared with the Japanese himawari-8/9 satellites. *Adv. Meteorol. Sci.* **2015**, *6*, 1–2016.
35. Min, M.; Wu, C.Q.; Li, C.; Liu, X.; Xu, N.; Wu, X.; Chen, L.; Wang, F.; Sun, F.; Qin, D.; et al. Developing the scienceproduct algorithm testbed for Chinese next-generation geostationary meteorological satellites: Fengyun-4 series. *J. Meteor. Res.* **2017**, *31*, 708–719. [[CrossRef](#)]
36. Cui, P.; Wang, S.J.; Lu, F.; Xiao, M. FY-4A/AGRI sea surface temperatures product and quality inspection. *J. Appl. Meteorol.* **2023**, *34*, 257–269. (In Chinese)
37. Li, Q.; He, Q.; Chen, C. Retrieval of daily mean VIIRS SST products in China seas. *Remote Sens.* **2021**, *13*, 5158. [[CrossRef](#)]
38. He, Q.J.; Hu, X.; Wu, Y.W. Evaluation and improvement of FY-4A/AGRI sea surface temperature data. *IEEE J. Sel. Top. Appl. Earth Obs. Remote Sens.* **2023**, *16*, 267–277. [[CrossRef](#)]
39. Wang, Y.Z.; Liu, H.L.; Zhang, Y.; Duan, M.Z.; Tang, S.H.; Deng, X.B. Validation of FY-4A AGRI layer precipitable water products using radiosonde data. *Atmos. Res.* **2021**, *253*, 105502. [[CrossRef](#)]
40. Xu, F.; Ignatov, A. In situ SST quality monitor (iQuam). *J. Atmos. Ocean. Technol.* **2014**, *31*, 164–180. [[CrossRef](#)]
41. He, X.W.; Xu, N.; Feng, X.H.; Hu, X.Q.; Xu, H.L.; Peng, Y. Assessing Radiometric Calibration of FY-4A/AGRI Thermal Infrared Channels Using CrIS and IASI. *IEEE Trans. Geosci. Remote Sens.* **2021**, *60*, 1–12. [[CrossRef](#)]
42. O’Carroll, A.G.; Eyre, J.R.; Saunders, R.W. Three-Way Error Analysis between AATSR, AMSR-E, and In Situ Sea Surface Temperature Observations. *J. Atmos. Ocean. Technol.* **2008**, *25*, 1197–1207. [[CrossRef](#)]
43. Gentemann, C.L. Three way validation of MODIS and AMSR-E sea surface temperatures. *J. Geophys. Res. Oceans* **2014**, *119*, 2583–2598. [[CrossRef](#)]
44. O’Carroll, A.G.; August, T.; Le Borgne, P.; Marsouin, A. The accuracy of SST retrievals from Metop-A IASI and A VHRR using the EUMETSAT OSI-SAF matchup dataset. *Remote Sens. Environ.* **2012**, *126*, 184–194. [[CrossRef](#)]

**Disclaimer/Publisher’s Note:** The statements, opinions and data contained in all publications are solely those of the individual author(s) and contributor(s) and not of MDPI and/or the editor(s). MDPI and/or the editor(s) disclaim responsibility for any injury to people or property resulting from any ideas, methods, instructions or products referred to in the content.